International Journal of Nanomedicine

Dovepress
Taylor & Francis Group

Open Access Full Text Article

ORIGINAL RESEARCH

Bionic Power Play: Dual-Targeting MDMX/MDM2 to Reboot p53 to Beat Lung Adenocarcinoma's Immune Tricks

Solomon Wong[1,*], Lu Xu[2,*], Weiming You[3,4], Wangxiao He[4], Xiaoqiang Zheng[4,5], Zhongquan Qi[1,6]

[1]School of Medicine, Guangxi University, Nanning, 530004, People's Republic of China; [2]Department of Physiology, Xiamen Medical College, Xiamen, 361023, People's Republic of China; [3]Department of Hepatology, The Second Affiliated Hospital of Xi'an Jiaotong University, Xi'an, 710004, People's Republic of China; [4]Department of Medical Oncology, The First Affiliated Hospital of Xi'an Jiaotong University, Xi'an, 710061, People's Republic of China; [5]Institute for Stem Cell and Regenerative Medicine, The Second Affiliated Hospital of Xi'an Jiaotong University, Xi'an, 710004, People's Republic of China; [6]Fujian Provincial Sperm Bank, Fujian Maternity and Child Health Hospital, Fuzhou, 350001, People's Republic of China

*These authors contributed equally to this work

Correspondence: Xiaoqiang Zheng; Zhongquan Qi, Email zhengxiaoqiang@xjtu.edu.cn; yxyyz@gxu.edu.cn

Background and Aim: MDM2 and MDMX are key regulators of the tumor suppressor p53 and are implicated in immune escape mechanisms in lung adenocarcinoma. Overexpression of these proteins inhibits p53 activity, limiting the immune system's ability to recognize and clear tumor cells, contributing to resistance against immune checkpoint inhibitors (ICIs). This study introduces a novel bionic peptide nanodrug, E@MDP, designed to target both MDM2 and MDMX, reactivate p53, and enhance the effectiveness of PD-1 immune checkpoint therapy in lung cancer.

Methods: E@MDP is constructed using a gold-mediated self-assembly method to form peptide-loaded nanoparticles, which are then encapsulated in erythrocyte membranes, enhancing stability and cell penetration. The physicochemical properties of the bionic nanodrug were evaluated, and its therapeutic efficacy was validated in vitro in LLC cells and in vivo using a syngeneic subcutaneous lung adenocarcinoma mice model.

Results: In vitro, E@MDP reinstated functional p53 activity, demonstrating a 2.46-fold upregulation compared to control groups, and significantly promoted tumor cell apoptosis, exhibiting a 3.9-fold enhancement. In vivo, E@MDP potentiated PD-1 checkpoint blockade by reprogramming the tumor immune microenvironment, ultimately driving a nearly two-fold enhancement in tumor regression versus monotherapies. Importantly, the E@MDP nanodrug exhibited favorable safety profiles, with no significant toxicity observed in preclinical models.

Conclusion: The E@MDP is a promising strategy for lung cancer immunotherapy and overcomes several limitations of conventional peptide drugs. The bionic nanodrug platform holds great potential for broader applications in cancers characterized by immune evasion.

Keywords: lung adenocarcinoma, immunotherapy, MDM2/MDMX, peptide, nanomedicine

Introduction

MDM2 and MDMX are key regulators of p53,[1] often engaged in immune escape mechanisms in a number of cancers, such as lung adenocarcinoma.[2,3] MDM2 and MDMX have been shown to suppress p53 activity, thereby limiting the immune system from effectively recognizing and clearing tumor cells.[4,5] Specifically, in wild-type p53 lung adenocarcinomas, MDM2/MDMX overexpression promotes immune escape, thereby conferring resistance to immune checkpoint inhibitors like ICIs.[6–8] Mechanistically, MDM2/MDMX upregulation suppresses p53-dependent pathways involved in antigen presentation, interferon signaling, and the expression of key chemokines, thereby impairing major histocompatibility complex class I expression and reducing T cell infiltration and activation within the tumor.[9,10] This results in

Received: 8 April 2025
Accepted: 4 August 2025
Published: 13 August 2025

a "cold" immunosuppressive microenvironment that limits the efficacy of PD-1/PD-L1 blockade. Moreover, MDM2 amplification has been clinically associated with hyperprogressive disease (HPD) following ICI treatment, highlighting its role in driving immune resistance and rapid tumor progression.[11,12]

Recent studies have established that MDM2/MDMX inhibition sensitizes tumors to immune checkpoint inhibition, enhancing therapeutic responses.[6,13] In lung cancer models, for instance, MDM2 and MDMX inhibition have been associated with p53 activity restoration,[14,15] which improves tumor repression and immune system reactivation.[16,17] These findings underscore the value of MDM2/MDMX targeting in wild-type p53 lung adenocarcinomas as a viable strategy to enhance the effectiveness of immunotherapy.[15,16] The design and synthesis of inhibitors with the capability to simultaneously target MDM2 and MDMX thus constitute a landmark breakthrough in overcoming immune resistance and increasing the general effectiveness of cancer immunotherapy. The development of dual-functional MDM2/MDMX inhibitors has been a topic of particular interest.[18–20] Small molecules have had some success in inhibiting MDM2, but dual inhibition of MDM2 and MDMX with these molecules has proved to be a challenge.[21–23] Peptide inhibitors, on the other hand, offer a viable alternative because they can efficiently target both proteins.[6,24,25] Peptides, however, suffer from limitations in terms of application in the clinic due to stability, susceptibility to enzymatic cleavage, and poor cell uptake.[26] In particular, peptides can be cleaved enzymatically and have poor cell membrane penetration.[27–29] To overcome these limitations, new strategies have to be designed, such as making membrane-penetrating[30–33] stable peptides. Building upon this, erythrocyte membrane-based biomimetic drug delivery systems offer a viable solution to the delivery challenges facing peptide therapeutics.[34,35] The presence of CD47 molecules on the erythrocyte membrane surface provides a "self-recognition" signal, enabling the coated nanoparticles to evade clearance by the immune system, thereby significantly prolonging their circulatory half-life and enhancing bioavailability. Additionally, the inherent barrier structure of the erythrocyte membrane effectively protects the encapsulated peptides from enzymatic degradation, further improving their stability and facilitating their accumulation within tumor tissues.[36,37] This would considerably enhance the therapeutic potential of peptide-based drugs, particularly in cancer immunotherapy, in which immune escape mechanisms in the tumor have to be overcome in order to achieve successful therapy.[36,38]

Herein, a new strategy to enhance the efficacy of peptide-based MDM2/MDMX inhibition in lung cancer therapy has been reported. We designed a bionic nanodrug, E@MDP, using a supramolecular self-assembly method mediated by a gold (Au) to construct peptide-loaded nanoparticles (NPs-MDP).[39,40] The nanoparticles were then encapsulated with erythrocyte membranes to give the system enhanced stability and cell membrane penetration.[38] The E@MDP nanodrug not only efficiently targets and inhibits MDM2 and MDMX but also restores p53 activity in lung adenocarcinoma cells and sensitizes tumors to PD-1 immune checkpoint inhibition. Our results indicate that this new drug efficiently activates the p53 pathway, induces apoptosis in tumor cells, and significantly enhances the therapeutic effect of immunotherapy in preclinical models. This strategy represents a tremendous breakthrough in overcoming the limitations of traditional peptide delivery systems and offers a novel and promising avenue for lung cancer therapy.

Materials and Methods

Preparation of NPs-MDP

This study employed the Fmoc-protected solid-phase synthesis strategy, utilizing the CS-BION336X fully automated peptide synthesis system, to prepare the target peptide following routine procedures established in prior research.[6,26] Then, NPs-MDP was prepared via a one-pot self-assembly method.[41] First, 2 mg of MDMX/MDM2 antagonistic peptide was dissolved in a mixed solvent of 0.5 mL ethanol and 1.25 mL ultrapure water. This was then mixed with a precursor solution of chloroauric acid (1 mL, 10 mM $HAuCl_4 \cdot xH_2O$), a thiolated PEG linker (0.5 mL, 4 mg/mL NH_2-PEG_{2000}-SH), and a HEPES buffer (2.25 mL, 100 mM, pH 7.0), and stirred under heating. Afterward, the mixture was combined with 2.25 mL ddH_2O and 2.25 mL of the HEPES buffer (100 mM, pH 7.0) and stirred at 70°C.

Preparation of E@MDP

E@MDP was prepared using a hypotonic lysis-membrane reconstitution technique to coat the peptide prodrug with erythrocyte membranes.[38] Blood was collected from the apex of the heart of C57BL/6 mice and treated with sodium

heparin as an anticoagulant. After differential centrifugation (3800×g, 10 min, 4°C) to remove plasma and granulocyte layers, the red blood cells were subjected to three washes in pre-cooled PBS (3000×g, 10 min, 4°C). Then, cells were lysed in hypotonic buffer at 4°C (12~16 h), followed by ultracentrifugation (13800×g, 15 min, 4°C) to remove hemoglobin and wash the membrane four times with PBS, resulting in a high-purity red blood cell membrane suspension. The erythrocyte membrane was mixed with NPs-MDP and sonicated (2 min, on/off ratio of 1:1000) to promote physical adsorption. The mixture was subsequently extruded through 200 nm and 50 nm polycarbonate membranes to achieve homogeneous membrane coating, followed by 0.22 μm filtration and storage in PBS at 4°C.

Characterization of E@MDP

The morphology and membrane integrity of E@MDP and NPs-MDP were observed by transmission electron microscopy (TEM) after the samples were loaded onto carbon-coated copper grids and stained with 2% phosphotungstic acid. The hydrodynamic diameter of the nanoparticles was measured using dynamic light scattering (DLS) to assess the effect of membrane modification on the particle size distribution. SDS-PAGE was performed to verify the integration of membrane proteins. RBC membranes, E@MDP, and NPs-MDP samples were treated with reducing sample buffer and separated on a 12% SDS-PAGE gel under constant voltage, followed by silver staining (Biyuntian, P0017S) and image acquisition.

Cellular Uptake and Intracellular Distribution Analysis

LLC cells were seeded into 6-well plates at a density of 2×10^5 cells per well. After the cells adhered completely, they were incubated with FITC-labeled E@MDP for 6 hours. Subsequently, the cells were harvested, and the uptake efficiency was quantitatively assessed by flow cytometry. For visualization of intracellular distribution, LLC cells were cultured in confocal microscopy dishes at a density of 1×10^5 cells per dish and incubated overnight. Drug intervention was performed as described above. The cells were then fixed with 4% paraformaldehyde, permeabilized using 0.1% Triton X-100, and stained with 4′,6-diamidino-2-phenylindole (DAPI) to visualize nuclei. The subcellular localization of E@MDP was subsequently examined using confocal laser scanning microscopy (CLSM).

Cell Culture and Cytotoxicity Assay

LLC cells (obtained from the Shanghai Cell Bank of the Chinese Academy of Sciences) were cultured in high-glucose DMEM medium supplemented with 10% heat-inactivated fetal bovine serum (37°C, 5% CO_{2o}). In the cytotoxicity assay, cells were seeded at a density of 3×10^3 cells per well in 96-well plates and incubated for 12 hours to allow for attachment. After replacing the medium with a fresh culture containing gradient concentrations of E@MDP, the cells were cultured for 24, 48, and 72 hours. The intervention was terminated, the medium was discarded, and 100 μL of Alamar Blue reagent (10% in DMEM medium) was added to each well. After 4 hours of incubation at 37°C in the dark, fluorescence intensity was measured using a microplate reader, and cell viability was quantified by relative fluorescence units (RFU).

Apoptosis Assay

LLC cultures at log-phase expansion were plated in 6-well clusters. Post-adhesion confirmation, E@MDP exposure was initiated for 24h, 48h, and 72h duration. Harvested cells underwent triple PBS washing cycles followed by centrifugal pelleting. Subsequent resuspension in binding buffer achieved 1×10^6 cells/mL density. Aliquots (100 μL) were sequentially stained with Annexin V-FITC (5 μL, 15 min, dark incubation) and PI (5 μL, 5 min, dark treatment), followed by buffer supplementation to a final volume of 500 μL. Cellular apoptosis profiles were immediately acquired through flow cytometric analysis using standardized acquisition parameters.

Immunofluorescence Assay of Cells

LLC cultures at log-phase expansion were plated in 35 mm imaging dishes (Thermo Scientific Nunc) under standard culture conditions (37°C, 5% CO_{2o}) for 12 h adhesion. Following 48 h E@MDP exposure, cells underwent sequential processing: immobilization in 4% PFA (15 min), membrane permeabilization with 0.1% Triton X-100 (10 min), and

nonspecific blocking using 5% BSA (1 h) at Room Temperature (RT). Primary antibodies against p53 (Santa Cruz, sc-126, 1:100), MDM2 (Abcam, ab259265, 1:100), and MDMX (Proteintech, 17914-1-AP, 1:100) were applied at 4°C for 16 h. After PBS washing cycles, species-matched Alexa Fluor-conjugated secondary antibodies (1:5000) were incubated under dark conditions (RT, 1 h), followed by DAPI nuclear counterstaining (5 min). Multiplex fluorescence signals were acquired using an Olympus FV3000 confocal system.

Animal Model Construction

C57BL/6 mice (aged 5–6 weeks) received subcutaneous engraftment with 8×10^5 LLC cells in the buttock region. Tumor progression was quantified through bidimensional caliper tracking, with randomization into three therapeutic cohorts initiated when lesion volumes attained 50–100 mm^3: control, E@MDP monotherapy (2 mg/kg, intravenous injection via tail vein (i.v)), E@MDP combined with anti-PD-1 (5 mg/kg, i.v. as previously described). At humane endpoints, specimens underwent systematic necropsy with tumor resection for histopathological evaluation using standardized protocols for hematoxylin-eosin (H&E) morphology, terminal deoxynucleotidyl transferase dUTP nick-end labeling (TUNEL), and immunohistochemistry (IHC) with validated scoring systems.

H&E Staining and Immunohistochemistry

Post-resection tumor specimens were processed through sequential histopathological protocols: 24 h immobilization in 4% paraformaldehyde, gradient ethanol dehydration, and paraffin embedding. Tissue sections were processed for H&E staining following conventional histological procedures. For Immunohistochemistry, tumor sections underwent xylene deparaffinization and alcohol gradient rehydration, followed by heat-mediated antigen retrieval and 0.3% Triton X-100 permeabilization (20 min). After 2 h blocking with 10% normal goat serum (RT), sections were incubated (4°C, 16 h) with validated primary antibodies: Ki-67 (CST D358, 1:400), p53 (Proteintech 10442-1-AP, 1:200), MDMX (Proteintech 17914-1-AP, 1:200), and MDM2 (Abcam ab259265, 1:200). Following PBS washes, HRP-conjugated secondary antibodies (1.5 h, RT) enabled DAB chromogenic detection, with hematoxylin counterstaining and whole-slide digital scanning for image analysis.

Immunofluorescence Staining

After deparaffinization and antigen retrieval, tissue sections were subjected to blocking to prevent non-specific binding, followed by sequential incubation with primary antibodies and horseradish peroxidase (HRP)-conjugated secondary antibodies. Subsequently, a tyramide signal amplification (TSA) fluorescence detection system was applied, in which fluorescent dyes were covalently bound to target sites under the catalytic action of HRP. After each round of immunostaining, the antibody complexes were removed using heat-induced epitope retrieval or chemical stripping, enabling repeated cycles for multiplex labeling. Finally, cell nuclei were counterstained with 4',6-diamidino-2-phenylindole (DAPI). Primary antibodies: anti-CD3 (Servicebio Technology, GB111337, 1:4000), anti-CD8α (Servicebio Technology, GB 15068, 1:4000), anti-CD4 (Abcam ab288724, 1:100), anti-CD25 (Abcam ab231441, 1:100).

TUNEL Staining

TUNEL staining was performed on paraffin sections after deparaffinization and rehydration. Sections were incubated with proteinase K to expose DNA ends. The TUNEL reaction mixture was applied to label DNA breaks. After washing, HRP-conjugated antibodies were used, and apoptotic cells were visualized by DAB staining. Sections were counterstained with hematoxylin and mounted for digital pathology scanning.

Safety Assessment

C57BL/6 mice were randomly assigned to control, E@MDP, and combination treatment groups (E@MDP + Anti-PD-1). Body weight changes were monitored daily to evaluate systemic toxicity. After the treatment period, blood samples were collected for complete blood cell counts and serum ALT, AST, urea nitrogen, and creatinine levels to assess liver and kidney toxicity. Upon euthanasia, major organs were harvested, and tissue sections were stained with H&E for histopathological analysis using a digital pathology scanner.

Statistical Analysis

Quantitative data are expressed as mean values with variability indicated by standard deviation (mean ± SD or Mean ±SE). Two-tailed Student's *t*-test and one-way ANOVA with Tukey's multiple comparison tests were applied to statistical differences between groups. Statistical significance thresholds were defined as: *P < 0.05 (significant), **P < 0.01 (highly significant), and ***P < 0.001 (extremely significant).

Results

Design and Construction of the Peptide Prodrug E@MDP

We initially utilized a previously developed intracellular-targeting peptide for the oncogenic proteins MDM2/MDMX and employed an Au-mediated one-step nanostructure self-assembly strategy to obtain nano-microprotein NPs-MDP. Simultaneously, erythrocyte membranes were extracted using a hypotonic centrifugation method, followed by multiple extrusions through a homogenizer, ultimately achieving the bionic nanomaterial E@MDP with erythrocyte membrane coating. This bionic peptide nanodrug E@MDP effectively targets intracellular MDM2/MDMX, alleviates their negative regulatory effects on p53, and promotes the reaccumulation of p53 within lung adenocarcinoma cells. It exerts anti-tumor effects while synergistically enhancing the efficacy of PD-1 inhibitor immunotherapy (Figure 1).

Physicochemical Characterization of E@MDP

We proceeded with the physicochemical characterization of E@MDP. Transmission Electron Microscopy (TEM) images (Figure 2A) revealed that NPs-MDP were relatively uniform spherical nanoparticles (approximately 20 nm in diameter). After erythrocyte membrane coating, E@MDP formed a typical core-shell structure, with the nanoparticle surface displaying a membrane structure, indicating successful erythrocyte membrane encapsulation (Figure 2B). Dynamic Light Scattering (DLS) measurements showed that the hydrodynamic diameter of NPs-MDP was approximately 21.04 nm, while that of E@MDP increased to 28.21 nm (Figure 2C). This change in particle size was consistent with the TEM

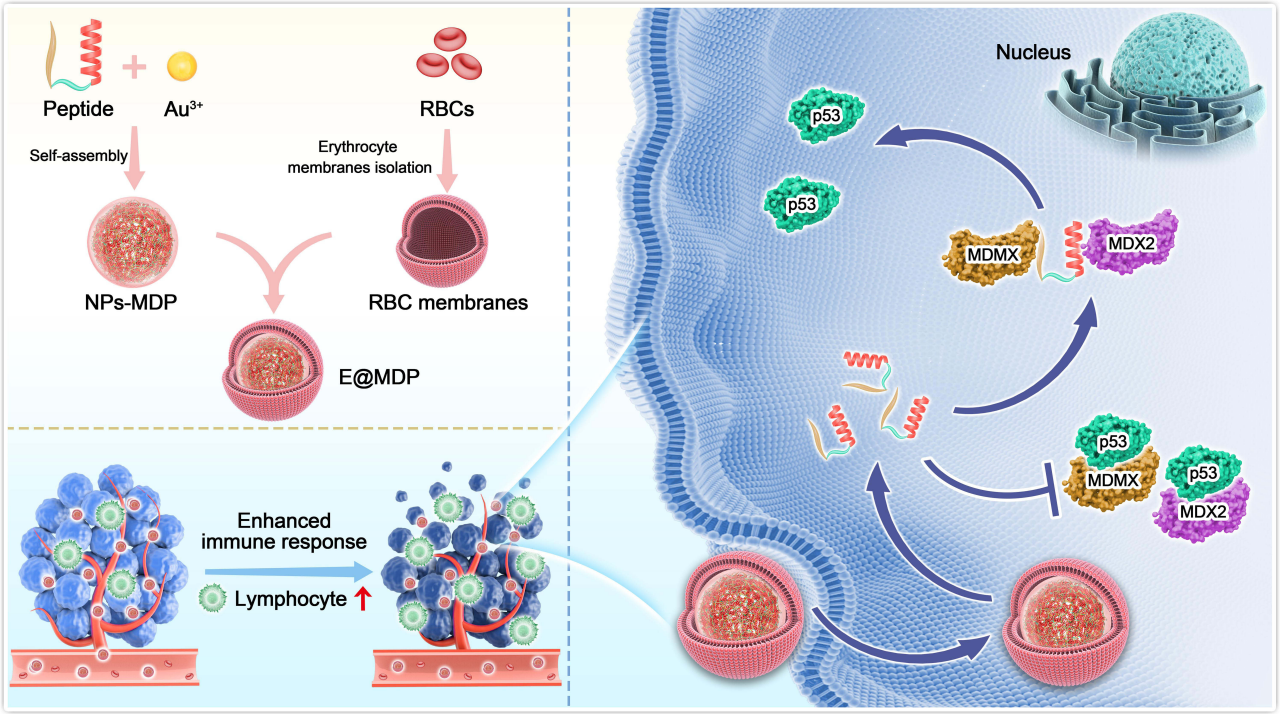

Figure 1 Schematic of E@MDP construction and function. We constructed the NPs-MDP precursor using Au(I)-mediated self-assembly to target and inhibit MDM2 and MDMX. Erythrocyte membrane coating led to the formation of the bionic peptide prodrug E@MDP. E@MDP effectively inhibits intracellular oncogenic proteins MDM2/MDMX, relieving their negative regulation on p53, restoring its tumor-suppressive function, and enhancing the efficacy of PD-1-based immunotherapy.

https://doi.org/10.2147/IJN.S533208

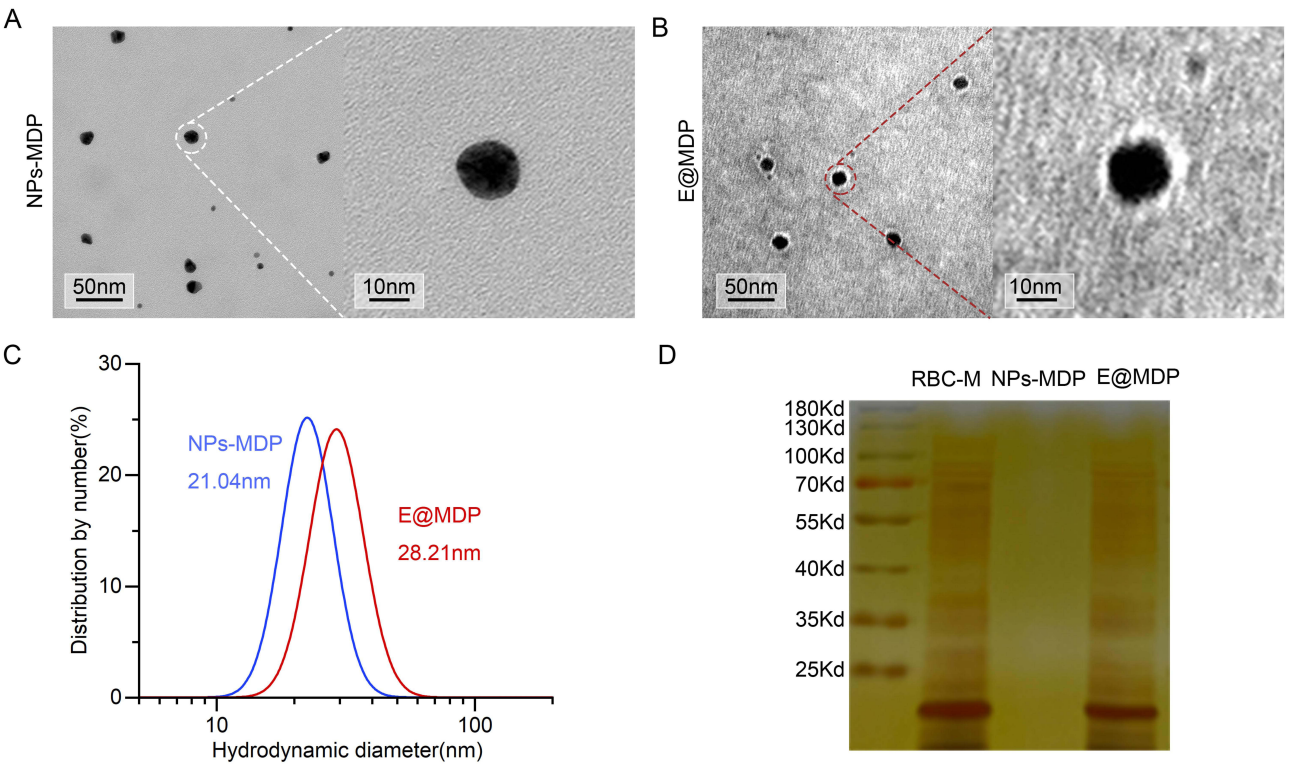

Figure 2 Characterization of E@MDP. (**A** and **B**) TEM images of NPs-MDP (**A**) and E@MDP (**B**); (**C**) DLS test of NPs-MDP and E@MDP; (**D**) SDS-PAGE silver staining for protein analysis of natural erythrocyte membranes (RBC-M), NPs-MDP, and E@MDP.

results, further validating the successful membrane coating. To confirm the protein composition of the membrane layer, we performed SDS-PAGE followed by silver staining (Figure 2D). The results indicated that the protein bands of E@MDP were highly consistent with those of natural erythrocyte membranes (RBC-M), while no significant protein bands were observed in NPs-MDP. This experiment confirmed that the surface of E@MDP retained the characteristic protein components of the erythrocyte membrane, establishing a bionic nanodelivery system.

Specifically, we performed flow cytometry analysis to assess the internalization efficiency of E@MDP in LLC cells quantitatively. The result revealed that the cellular uptake efficiency of E@MDP exceeded 90% (Figure S1A). In addition, confocal laser scanning microscopy (CLSM) was employed to visualize the intracellular distribution of E@MDP. As shown in Figure S1B, the FITC-labeled E@MDP was clearly observed within the cytoplasm of LLC cells, providing direct evidence of successful intracellular delivery. These results substantiate our claim regarding the enhanced intracellular delivery capability of E@MDP, which contributes to its improved antitumor efficacy.

Mechanism-Driven Antineoplastic Activity of E@MDP Through p53 Pathway Activation

To elucidate the underlying mechanism of the pharmacological activity of E@MDP, we conducted different evaluations using Lewis lung carcinoma (LLC) models. Cell viability assays demonstrated that E@MDP induced time- and dose-dependent cytotoxicity following 24, 48, and 72-hour treatments across the tested concentration range (0–13.1 μM). Quantitative analysis revealed that E@MDP effectively inhibited tumor cell proliferation, with calculated half-maximal inhibitory concentrations (IC_{50}) of 4.86 μM at 24 hours (Figure S2A), 1.96 μM at 48 hours (Figure 3A), and 0.91 μM at 72 hours (Figure S2B), respectively. Detailed flow cytometric analysis using Annexin V-FITC/PI dual staining provided mechanistic insights into the pro-apoptotic effects of E@MDP. Comparative analysis indicated a marked elevation in apoptotic indices between the treatment groups and controls. Quantitative data showed a 6-fold increase in early apoptotic populations (Annexin V+/PI-) and a 2.7-fold increase in late apoptotic cells (Annexin V+/PI+) following

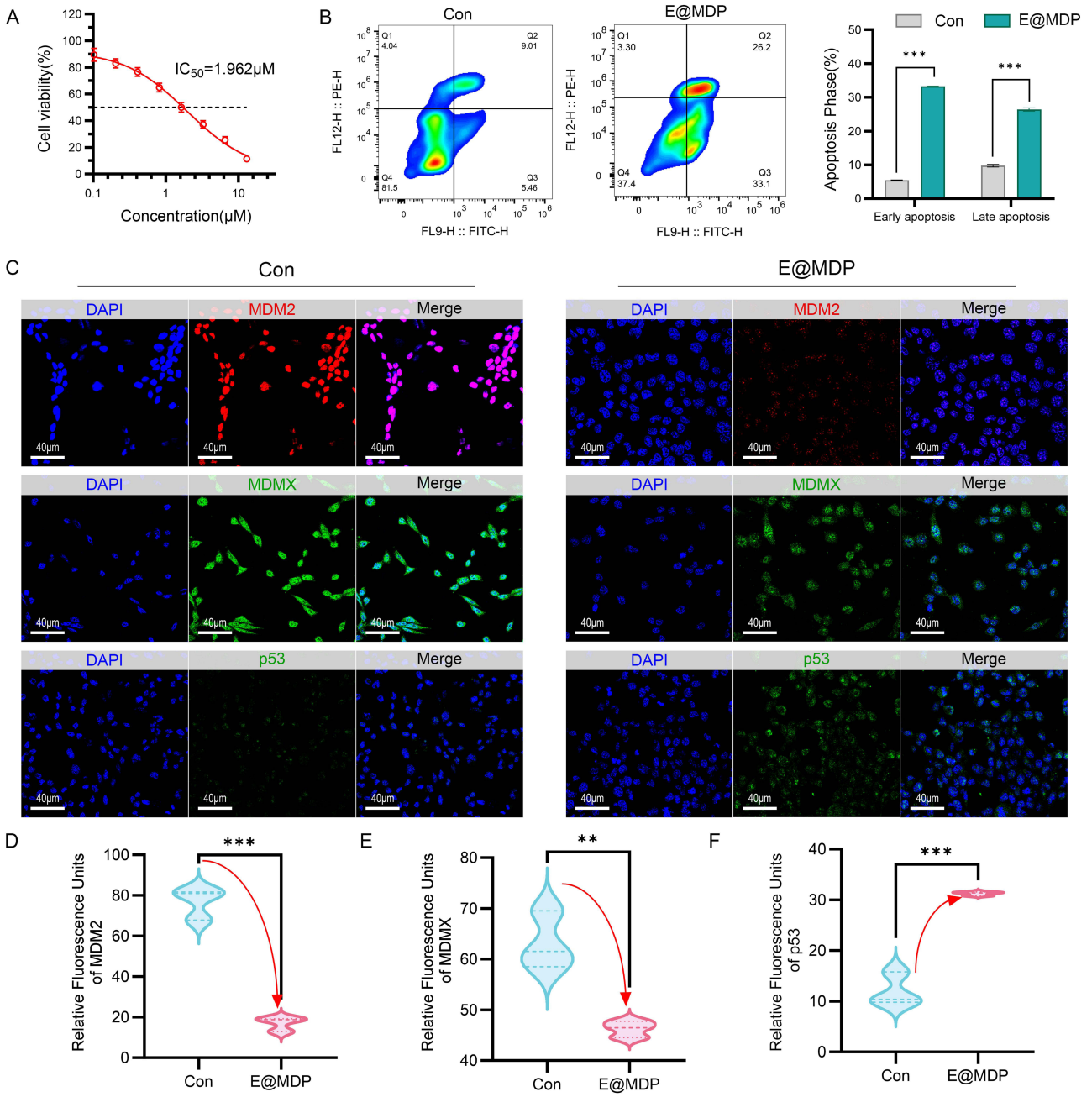

Figure 3 E@MDP activates the p53 pathway via targeted degradation of MDM2/MDMX for antitumor action. (**A**) The cytotoxic effect of E@MDP on LLC cells after 48 hours of treatment was assessed using the Alamar Blue assay (n=3). (**B**) Flow cytometry analysis of apoptosis in LLC cells treated with E@MDP for 48 hours (n=3). (**C**–**F**) Immunofluorescence (**C**) and relative fluorescence quantification analysis of MDM2 (**D**), MDMX (**E**), and p53 (**F**) protein expression in LLC cells after 48 hours of E@MDP treatment (n=3). (**p < 0.01, ***p < 0.001).

E@MDP administration (Figure 3B). These findings support the conclusion that activation of the p53-mediated pathway is a principal mechanism underlying the tumor-suppressive effects of E@MDP.

To delineate the molecular underpinnings of E@MDP's antitumor efficacy, quantitative cellular immunofluorescence analysis was conducted to interrogate its regulatory impact on the MDM2/MDMX-p53 signaling axis within p53-competent LLC cellular models. After 48 hours of E@MDP treatment, cells were fixed and labeled with anti-MDM2 (red fluorescence), anti-MDMX (green fluorescence), and anti-p53 (green fluorescence) antibodies, with DAPI used for nuclear staining. Fluorescence intensity quantification was performed using ImageJ. As shown in Figure 3C and D, MDM2 exhibited significant nuclear accumulation in the Control group LLC cells (red fluorescence). After E@MDP

https://doi.org/10.2147/IJN.S533208

treatment, the nuclear fluorescence intensity of MDM2 decreased by 77.9% compared to the Control group. Concurrently, the fluorescence intensity of MDMX was reduced by 26.8% in the treatment group (Figure 3C and E), suggesting that E@MDP can simultaneously target and inhibit the expression levels of MDM2/MDMX. Further analysis of p53 protein expression (Figure 3C and F) showed low basal expression of p53 in the Control group, while E@MDP treatment significantly increased the p53 protein level, with fluorescence intensity 2.6 times higher than the Control group, indicating that E@MDP restores the accumulation of p53 in lung adenocarcinoma cells. These results suggest that E@MDP, by dual-targeting MDM2/MDMX, alleviates their negative regulation of p53 and promotes its functional accumulation in the nucleus, exerting anti-lung adenocarcinoma effects.

Activation of the p53 Pathway Through Targeted Degradation of MDM2/MDMX by E@MDP for Antitumor Action

As depicted in Figure 4A, a subcutaneous xenograft mouse model of lung adenocarcinoma was established by injecting 8×10^5 LLC cells into the subcutaneous tissue of the mice's buttock regions. Following randomization, experimental cohorts comprised: vehicle control receiving PBS, E@MDP monotherapy (2 mg/kg, i.v), and combinatorial treatment with concurrent E@MDP administration (2 mg/kg) plus PD-1 immune checkpoint blockade (Anti-PD-1, 5 mg/kg, i.v). The treatment was administered every three days for a total of five cycles. Following therapeutic protocols, animals underwent humane sacrifice with subsequent tumor resection for photographic documentation (Figure 4B). The E@MDP group exhibited a significantly reduced tumor volume compared to the control group, with the combination treatment group demonstrating an even more substantial inhibition of tumor growth. The tumor volume growth curves followed a similar trend, with E@MDP significantly inhibiting LLC xenograft growth with an inhibition rate of 22.3%, while the combination therapy group showed nearly a two-fold increase in inhibition rate, reaching 43.1% compared to the single-agent group (Figure 4C). Tumor weight analysis also revealed that the inhibition rate for the E@MDP single-agent group was 38.7%, while the combined treatment group achieved a 65.5% tumor suppression rate (Figure 4D). Hematoxylin-eosin (HE) staining of the tumor tissues confirmed the results (Figure 4E).

To evaluate the therapeutic efficacy of E@MDP in vivo, we conducted comprehensive histological analyses of tumor specimens. TUNEL assays revealed significant apoptosis induction across treatment groups, with the E@MDP monotherapy cohort exhibiting a 3.2-fold increase in apoptotic index compared to control, and combination therapy achieved a 5.45-fold elevation (Figure 4F). These findings substantiate that E@MDP effectively triggers apoptotic pathways of lung tumor in vivo, contributing to tumor volume reduction. Complementary Ki-67 immunohistochemical analysis demonstrated marked suppression of this proliferation marker in E@MDP-treated tumors, corroborating the prodrug's dual mechanism of action in both inhibiting cellular proliferation and promoting apoptosis.

Mechanistic investigations through protein expression profiling showed substantial downregulation of MDM2/MDMX oncoproteins following E@MDP administration. H-score analysis indicated that compared to the control group, MDM2 and MDMX scores were reduced by 96.5% and 48.1% in the E@MDP group, respectively, and by 95.7% and 44.8% in the combination treatment group, with no significant difference between the two treatment groups (Figure 4F). Similarly, E@MDP treatment significantly increased p53 protein expression in tumor cells, with H-score analysis showing a 5.89-fold increase in the E@MDP group and a 5.66-fold increase in the combination treatment group (Figure 4F).

To further elucidate the immunomodulatory role of E@MDP in reshaping the tumor microenvironment, we performed immunofluorescence staining to analyze immune cell infiltration within tumor tissues. As illustrated in Figure S3, E@MDP treatment significantly increased the infiltration of $CD3^+/CD8^+$ cytotoxic T lymphocytes, with approximately a seven-fold elevation observed in the combination treatment group compared to controls (Figure S3A). Concurrently, the proportion of immunosuppressive $CD4^+/CD25^+$ regulatory T cells (Tregs) was substantially reduced (Figure S3B). These results suggest that E@MDP effectively reactivates the p53 signaling pathway, enhancing T cell-mediated antitumor immunity while simultaneously mitigating Treg-driven immunosuppression. Collectively, our findings highlight that E@MDP not only exerts direct antitumor effects through dual MDM2/MDMX inhibition and p53

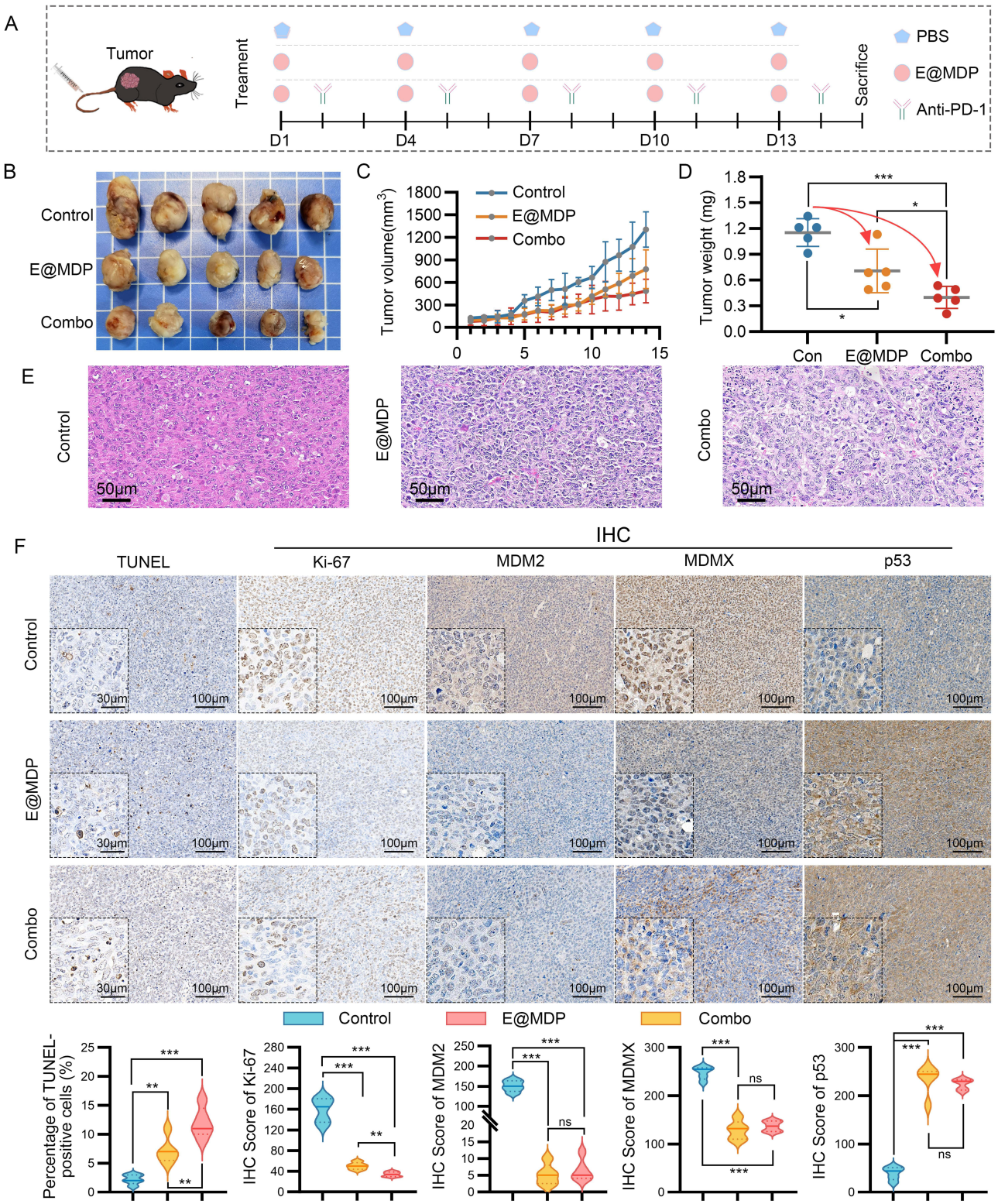

Figure 4 E@MDP effectively activates the p53 pathway and exerts antitumor activity in a lung adenocarcinoma mouse xenograft model, with enhanced synergy with anti-PD-1 immunotherapy. (**A**) Schematic of the mouse model construction and drug administration. (**B**) Tumor tissue images of mice after treatment. (**C**) Tumor volume growth curve. (**D**) Tumor weight analysis. (**E**) HE staining of tumor tissues (scale bar: 50 μm). (**F**) TUNEL staining and quantification, Ki-67, MDM2, MDMX, and p53 immunohistochemical staining and immunohistochemical scoring (scale bar: 30 μm, 100 μm). (*p < 0.05, **p < 0.01, ***p < 0.001, ns, no significant difference).

https://doi.org/10.2147/IJN.S533208

pathway reactivation but also profoundly remodels the immunosuppressive landscape of the tumor microenvironment, thus synergistically augmenting the therapeutic efficacy of PD-1-based immune checkpoint blockade.

Safety Evaluation of E@MDP

We evaluated the biosafety of E@MDP. Body weight, an important indicator of the nutritional and health status of mice, was monitored during the treatment period (Figure 5A). The results showed that the body weight of animals in all three

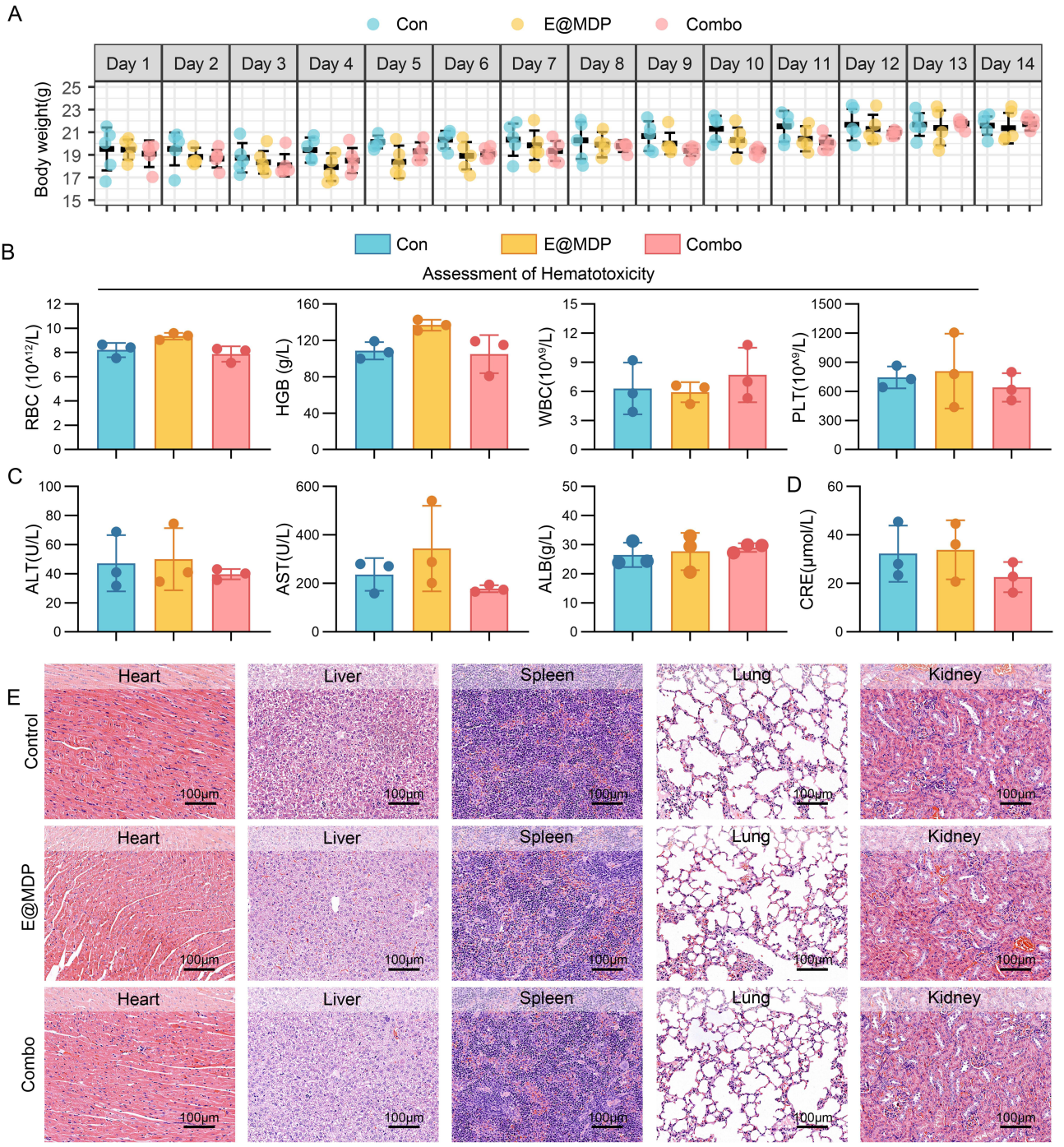

Figure 5 In vivo safety evaluation of E@MDP. (**A**) Body weight changes in the treatment groups (n=5). (**B**) Complete blood count analysis of peripheral blood (n=3). (**C**) Liver function assessment with ALT, AST, and ALB levels (n=3). (**D**) Kidney function assessment via creatinine (CRE) levels (n=3). (**E**) Histopathological examination of heart, liver, spleen, lung, and kidney tissues after E@MDP intervention, with HE staining (scale bar: 100 μm).

groups maintained normal growth curves, with no significant differences between the groups, indicating that E@MDP monotherapy and the combination treatment did not induce systemic toxicity. We also collected peripheral blood from mice for complete blood count and liver/kidney function assessments. As shown in Figure 5B, the blood cell counts, including red blood cells (RBC), hemoglobin (HGB), white blood cells (WBC), and platelet count (PLT) levels, remained within the normal physiological range, suggesting that E@MDP and its combination with Anti-PD-1 did not cause significant bone marrow suppression. Liver function analysis (Figure 5C) showed that serum ALT, AST, and ALB levels were within normal metabolic ranges, with no significant liver toxicity observed. Likewise, no significant increase in endogenous creatinine (CRE) levels, a marker of renal function, was observed in the kidney function tests (Figure 5D). These results suggest that E@MDP and its combination with Anti-PD-1 did not induce significant hematological, liver, or kidney toxicity. Additionally, histopathological examination of various organs (heart, liver, spleen, lungs, and kidneys) showed no significant structural abnormalities or pathological changes in any group, as assessed by H&E staining (Figure 5E). These comprehensive data demonstrate that the combination of E@MDP and PD-1 inhibitors offers significant antitumor efficacy without increasing toxicity, providing a promising and safe therapeutic strategy for future clinical translation.

Discussion

This study provides useful insight into the design of a bionic peptide nanodrug (E@MDP) that effectively targets MDM2 and MDMX, two major inhibitors of p53 activity in lung adenocarcinoma. Through a strategy involving a gold-mediated self-assembly method to construct peptide-loaded nanoparticles and then encapsulate them with erythrocyte membranes,[42,43] we were able to enhance drug stability and cell uptake. This drug not only restores p53 activity by suppressing both MDM2 and MDMX, but it also greatly enhances the efficacy of PD-1 inhibitor immunotherapy, with a definite synergistic effect between the nanodrug and immunotherapy. These findings offer a potential strategy to overcome immune resistance in lung cancer and may have broad applications in treating other cancers with a similar immune escape mechanism.

The successful design and synthesis of E@MDP prove that cell membrane-derived nanoparticles have great potential in targeted drug delivery system design. Through using erythrocyte membranes, a bionic nanodrug has been designed with the ability to overcome many of the common obstacles to conventional peptide drugs, such as degradation and poor cell penetration.[36] The membrane coating not only stabilizes the drug but also enables targeted delivery to cancer cells, with higher therapeutic concentrations at the target location. This approach represents a breakthrough in peptide-based drugs and offers a practical solution to drug stability and delivery issues. Additionally, being able to target and inhibit both MDM2 and MDMX with a single, bi-functional drug may result in more effective treatments for a number of cancers, particularly those that have developed resistance to conventional treatments.

The therapeutic implications for lung cancer therapy are considerable, as it addresses one of the key impediments to current therapeutic strategies: immune resistance to therapy induced by MDM2/MDMX. Through p53 reactivation and sensitization to PD-1 inhibitors, E@MDP provides an effective strategy to circumvent such resistance. However, despite these promising results, a variety of challenges remain. Firstly, further drug formulation and delivery system refinement will be needed to ensure successful clinical translation. Secondly, while results in animal models are promising, off-target activity and long-term toxicity have not been extensively evaluated. Finally, clinical trials will be needed to establish efficacy and safety in human patients. Regardless, this study identifies the possibility of using bionic nanodrugs to enhance cancer immunotherapy and provides a platform for future studies in this field, with a vision to ultimately enhance patient outcomes and advance personalized cancer therapeutic strategies.

Ethics Approval and Consent to Participate

All animal experiments were conducted in strict accordance with the National Institutes of Health Guide for the Care and Use of Laboratory Animals (NIH) and the Guidelines of the Biomedical Ethics Committee of Health Science Center of Xi'an Jiaotong University (Approval Number: 2021-1734).

Acknowledgments

We thank the Instrument Analysis Center of Xi'an Jiaotong University for their assistance with TEM and DLS analysis.

Funding

This research was funded by the National Natural Science Foundation of China (No.82303816).

Disclosure

The authors report no conflicts of interest in this work.

References

1. Peuget S, Zhou X, Selivanova G. Translating p53-based therapies for cancer into the clinic. *Nat Rev Cancer*. 2024;24(3):192–215. doi:10.1038/s41568-023-00658-3
2. Carlsen L, Zhang S, Tian X, et al. The role of p53 in anti-tumor immunity and response to immunotherapy. *Front Mol Biosci*. 2023;10:1148389. doi:10.3389/fmolb.2023.1148389
3. Blagih J, Buck MD, Vousden KH, Lennon-Duménil A-M. p53, cancer and the immune response. *J Cell Sci*. 2020;133(5):jcs237453. doi:10.1242/jcs.237453
4. Liu Y, Su Z, Tavana O, Gu W. Understanding the complexity of p53 in a new era of tumor suppression. *Cancer Cell*. 2024;42(6):946–967. doi:10.1016/j.ccell.2024.04.009
5. Khoo KH, Verma CS, Lane DP. Drugging the p53 pathway: understanding the route to clinical efficacy. *Nat Rev Drug Discovery*. 2014;13(3):217–236. doi:10.1038/nrd4236
6. Zheng X, Yan J, You W, et al. De novo nano-erythrocyte structurally braced by biomimetic Au(I)-peptide skeleton for MDM2/MDMX predation toward augmented pulmonary adenocarcinoma Immunotherapy. *Small*. 2021;17(20):e2100394. doi:10.1002/smll.202100394
7. Wang X, Wang F, Zhong M, Yarden Y, Fu L. The biomarkers of hyperprogressive disease in PD-1/PD-L1 blockage therapy. *Mol Cancer*. 2020;19(1):81. doi:10.1186/s12943-020-01200-x
8. Sun H, Liu SY, Zhou JY, et al. Specific TP53 subtype as biomarker for immune checkpoint inhibitors in lung adenocarcinoma. *EBioMedicine*. 2020;60:102990. doi:10.1016/j.ebiom.2020.102990
9. Zeng Q, Zeng S, Dai X, et al. MDM2 inhibitors in cancer immunotherapy: current status and perspective. *Genes Dis*. 2024;11(6):101279. doi:10.1016/j.gendis.2024.101279
10. Ingelshed K, Melssen MM, Kannan P, et al. MDM2/MDMX inhibition by Sulanemadlin synergizes with anti-programmed death 1 immunotherapy in wild-type p53 tumors. *iScience*. 2024;27(6):109862. doi:10.1016/j.isci.2024.109862
11. Champiat S, Dercle L, Ammari S, et al. Hyperprogressive disease is a new pattern of progression in cancer patients treated by anti-PD-1/PD-L1. *Clin Cancer Res*. 2017;23(8):1920–1928. doi:10.1158/1078-0432.Ccr-16-1741
12. Sun D, Qian H, Li J, Xing P. Targeting MDM2 in malignancies is a promising strategy for overcoming resistance to anticancer immunotherapy. *J Biomed Sci*. 2024;31(1). doi:10.1186/s12929-024-01004-x
13. Fang DD, Tang Q, Kong Y, et al. MDM2 inhibitor APG-115 synergizes with PD-1 blockade through enhancing antitumor immunity in the tumor microenvironment. *J ImmunoTher Cancer*. 2019;7(1):327. doi:10.1186/s40425-019-0750-6
14. Yang W, Liu W, Li X, Yan J, He W. Turning chiral peptides into a racemic supraparticle to induce the self-degradation of MDM2. *J Adv Res*. 2023;45:59–71. doi:10.1016/j.jare.2022.05.009
15. Yan J, Yao Y, Yan S, Gao R, Lu W, He W. Chiral protein supraparticles for tumor suppression and synergistic immunotherapy: an enabling strategy for bioactive supramolecular chirality construction. *Nano Lett*. 2020;20(8):5844–5852. doi:10.1021/acs.nanolett.0c01757
16. Brummer T, Zeiser R. The role of the MDM2/p53 axis in antitumor immune responses. *Blood*. 2024;143(26):2701–2709. doi:10.1182/blood.2023020731
17. Ghafoor NA, Yildiz A. Targeting MDM2–p53 axis through drug repurposing for cancer therapy: a multidisciplinary approach. *ACS Omega*. 2023;8(38):34583–34596. doi:10.1021/acsomega.3c03471
18. Yan J, Zheng X, You W, He W, Xu G-K. A Bionic-Homodimerization strategy for optimizing modulators of protein–protein interactions: from statistical mechanics theory to potential clinical translation. *Adv Sci*. 2022;9(11):e2105179. doi:10.1002/advs.202105179
19. Zhao X, Xiong D, Luo S, Duan L. Molecular investigation of the dual inhibition mechanism for targeted P53 regulator MDM2/MDMX inhibitors. *Phys Chem Chem Phys*. 2022;24(27):16799–16815. doi:10.1039/d2cp01780f
20. Duffy MJ, Synnott NC, O'Grady S, Crown J. Targeting p53 for the treatment of cancer. *Semin Cancer Biol*. 2022;79:58–67. doi:10.1016/j.semcancer.2020.07.005
21. Sun L, Liu H, Ye Y, et al. Smart nanoparticles for cancer therapy. *Signal Transduction Targeted Ther*. 2023;8(1):418. doi:10.1038/s41392-023-01642-x
22. Fan D, Cao Y, Cao M, Wang Y, Cao Y, Gong T. Nanomedicine in cancer therapy. *Signal Transduction Targeted Ther*. 2023;8(1):293. doi:10.1038/s41392-023-01536-y
23. Alaseem AM. Advancements in MDM2 inhibition: clinical and pre-clinical investigations of combination therapeutic regimens. *Saudi Pharm J*. 2023;31(10):101790. doi:10.1016/j.jsps.2023.101790
24. Chen S, Li X, Li Y, et al. Design of stapled peptide-based PROTACs for MDM2/MDMX atypical degradation and tumor suppression. *Theranostics*. 2022;12(15):6665–6681. doi:10.7150/thno.75444
25. Yang J, Li Y, Aguilar A, Liu Z, Yang CY, Wang S. Simple structural modifications converting a bona fide MDM2 PROTAC degrader into a molecular glue molecule: a cautionary tale in the design of PROTAC degraders. *J Med Chem*. 2019;62(21):9471–9487. doi:10.1021/acs.jmedchem.9b00846

26. He W, Yan J, Li Y, et al. Resurrecting a p53 peptide activator - An enabling nanoengineering strategy for peptide therapeutics. *J Control Release*. 2020;325:293–303. doi:10.1016/j.jconrel.2020.06.041
27. Chehelgerdi M, Chehelgerdi M, Allela OQB, et al. Progressing nanotechnology to improve targeted cancer treatment: overcoming hurdles in its clinical implementation. *Mol Cancer*. 2023;22(1):169. doi:10.1186/s12943-023-01865-0
28. Fang RH, Jiang Y, Fang JC, Zhang L. Cell membrane-derived nanomaterials for biomedical applications. *Biomaterials*. 2017;128:69–83. doi:10.1016/j.biomaterials.2017.02.041
29. Yan S, Yang W, You W, He W, Yan J, Yao Y. Resurrecting p53 by an artificial nano-protein for potent photodynamic retinoblastoma therapy. *Small*. 2024;21(4):e2401260. doi:10.1002/smll.202401260
30. He W, Zhang Z, Yang W, et al. Turing milk into pro-apoptotic oral nanotherapeutic: de novo bionic chiral-peptide supramolecule for cancer targeted and immunological therapy. *Theranostics*. 2022;12(5):2322–2334. doi:10.7150/thno.70568
31. Yong T, Wei Z, Gan L, Yang X. Extracellular-vesicle-based drug delivery systems for enhanced antitumor therapies through modulating the cancer-immunity cycle. *Adv Mater*. 2022;34(52):e2201054. doi:10.1002/adma.202201054
32. Tang Q, Sun S, Wang P, et al. Genetically engineering cell membrane-coated bto nanoparticles for mmp2-activated piezocatalysis-immunotherapy. *Adv Mater*. 2023;35(18):e2300964. doi:10.1002/adma.202300964
33. Jiang J, Cui X, Huang Y, et al. Advances and prospects in integrated nano-oncology. *Nano Biomed Eng*. 2024;16(2):152–187. doi:10.26599/NBE.2024.9290060
34. Liao J, Gong L, Xu Q, et al. Revolutionizing neurocare: biomimetic nanodelivery via cell membranes. *Adv Mater*. 2024;36(26). doi:10.1002/adma.202402445
35. Han X, Shen SF, Fan Q, et al. Red blood cell-derived nanoerythrosome for antigen delivery with enhanced cancer immunotherapy. *Sci Adv*. 2019;5(10). doi:10.1126/sciadv.aaw6870
36. Nguyen PHD, Jayasinghe MK, Le AH, Peng B, Le MTN. Advances in drug delivery systems based on red blood cells and their membrane-derived nanoparticles. *ACS Nano*. 2023;17(6):5187–5210. doi:10.1021/acsnano.2c11965
37. Xia Q, Zhang Y, Li Z, Hou X, Feng N. Red blood cell membrane-camouflaged nanoparticles: a novel drug delivery system for antitumor application. *Acta Pharmaceutica Sinica B*. 2019;9(4):675–689. doi:10.1016/j.apsb.2019.01.011
38. Jiang A, Zheng X, Yan S, Yan J, Yao Y, He W. Advancing the boundaries of immunotherapy in lung adenocarcinoma with idiopathic pulmonary fibrosis by a biomimetic proteinoid enabling selective endocytosis. *ACS Nano*. 2024;18(7):5358–5373. doi:10.1021/acsnano.3c09852
39. Yan S, Yan J, Liu D, et al. A nano-predator of pathological MDMX construct by clearable supramolecular gold(I)-thiol-peptide complexes achieves safe and potent anti-tumor activity. *Theranostics*. 2021;11(14):6833–6846. doi:10.7150/thno.59020
40. Wu Y, Zhang J, He W, Li C, Wang Y. Nanomaterials for targeting liver disease: research progress and future perspectives. *Nano Biomed Eng*. 2023;15(2):199–224. doi:10.26599/nbe.2023.9290024
41. Yan J, Ji F, Yan S, et al. A general-purpose nanohybrid fabricated by polymeric Au(I)-peptide precursor to wake the function of peptide therapeutics. *Theranostics*. 2020;10(19):8513–8527. doi:10.7150/thno.47243
42. Srivastava I, Xue R, Jones J, et al. Biomimetic surface-enhanced raman scattering nanoparticles with improved dispersibility, signal brightness, and tumor targeting functions. *ACS Nano*. 2022;16(5):8051–8063. doi:10.1021/acsnano.2c01062
43. Miao Y, Yang Y, Guo L, et al. Cell membrane-camouflaged nanocarriers with biomimetic deformability of erythrocytes for ultralong circulation and enhanced cancer therapy. *ACS Nano*. 2022;16(4):6527–6540. doi:10.1021/acsnano.2c00893